Journal of Molecular Structure 1350 (2026) 144049

Contents lists available at ScienceDirect

Journal of Molecular Structure

journal homepage: www.elsevier.com/locate/molstr

A multifunctional Schiff base: Investigating its Zirconium sensing capabilities and antiproliferative effects

Gurjaspreet Singh [a,*], Parul [a,*], Ankush Sheoran [b], Baljinder Singh Gill [c,*], Deepanjali Baliyan [c], Amarjit Kaur [a], Daizy Rani Batish [d], Aditi Rana [d], Brij Mohan [e]

[a] Department of Chemistry, Panjab University, Chandigarh 160014, India
[b] State Key Laboratory of Flexible Electronics (LoFE) & Institute of Advanced Materials (IAM), Nanjing Tech University, Jiangsu, China
[c] Department of Biochemistry, Central University of Punjab, Bathinda 151401, India
[d] Department of Botany, Panjab University, Chandigarh 160014, India
[e] Centro de Química Estrutural, Instituto Superior Técnico, Universidade de Lisboa (ULisboa), Av. Rovisco Pais1, 1049-001, Portugal

ARTICLE INFO

Keywords:
Schiff base
Indole-3-carboxaldehyde
Molecular docking
Anticancer
Zirconium(IV)

ABSTRACT

The current investigation is focused on the synthesis of indole-3-carboxaldehyde functionalized Schiff base 5, which was characterized via X-ray crystallographic study, ^{1}H NMR spectroscopy, ^{13}C NMR spectroscopy, FT-IR spectroscopy, mass spectrometry (LCMS) and thermal gravimetric analysis (TGA). Compound 5 has been identified as an effective and highly selective Zr(IV) sensor using UV–Visible spectroscopy with a limit of detection (LOD) 3.7×10^{-7} M. Compound 5 exhibited the most significant anticancer activity, reducing cell viability by upto 67.67 % compared to untreated control cells. Experiments on *Cajanus cajan* (pigeon pea) seeds revealed its efficacy as a good plant growth regulator. Molecular docking studies further supported its therapeutic potential by revealing strong interactions with both an anticancer target protein and a plant gibberellin protein, indicating its dual role as potential anticancer agent and a plant growth regulator. The findings from the study provides the foundation for future research into zirconium sensing and anticancer applications, potentially leading to the development of new sensors and anticancer drugs.

1. Introduction

The ongoing analysis centers on a Schiff base derived from indole-3-carboxaldehyde, demonstrating its efficacy as a selective chemosensor for zirconium(IV). Zirconium is a ubiquitous metal which finds widespread applications in different industries [1]. Its unique properties, such as hardness [2], thermal stability [3], high melting point [4], abrasiveness and antioxidant characteristics [5] make it valuable in sectors like paper printing, catalysis, cosmetics, paint industry and also acts as a catalyst [6–8]. In the nuclear industry, zirconium alloys are essential components in construction of pressure tubes and fuel channels [9]. Additionally, it has numerous uses in medical domain which includes dentures and prosthesis [10–12]. The diverse applications of zirconium highlight its importance on a variety of scales. But An overabundance of this element can have deleterious consequences encompassing various disorders including pulmonary pneumoconiosis, skin irritation, and granulomas which are brought on by excessive zirconium inhalation and extended exposure to the body [13,14]. Consequently, the accurate and timely detection of excess zirconium assumes paramount importance. Schiff bases, featuring the characteristic imine functional group exhibit a diverse array of properties across the board not only significant biological activities such as anticancer, antioxidants, antifungal and antimicrobial effects, but also a wide spectrum of other valuable characteristics [15–18]. Cancer is an ailment characterized by the uncontrolled accumulation and malignant transformation of cells [19]. These aberrant cells exhibit genetic mutations, enabling them to invade and damage surrounding tissues, compromising the integrity of vital bodily functions [20,21]. The number of cancer patients worldwide are increasing at a very quick pace, making the treatment of cancer cells crucial [22–24]. The development of new anticancer agents is vital for improved cancer treatment outcomes [25]. Schiff bases can also be used as regulators of plant development and have demonstrated efficacy as plant growth regulators [26].

Plant growth regulators are a class of organic compound which have ability to stimulate, impede, or alter a variety of physiological processes in plants, including stimulation, inhibition and alteration [27]. They

* Corresponding authors.
E-mail addresses: gjpsingh@pu.ac.in (G. Singh), parul029r@gmail.com (Parul), baljindersingh@cup.edu.in (B.S. Gill).

https://doi.org/10.1016/j.molstruc.2025.144049
Received 12 June 2025; Received in revised form 13 September 2025; Accepted 16 September 2025
Available online 16 September 2025

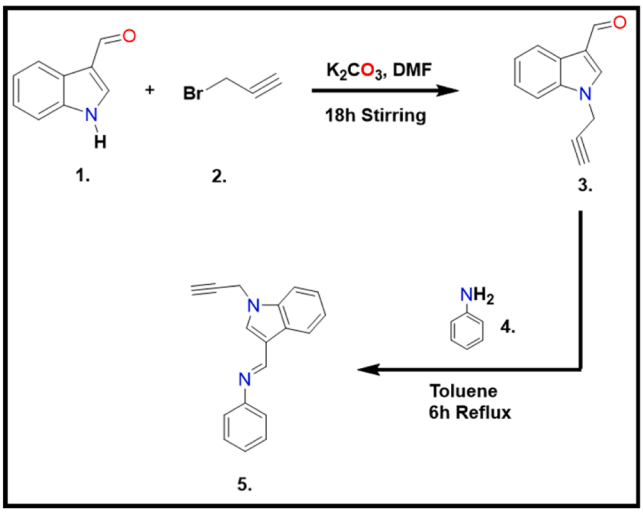

Scheme 1. Synthesis of 5.

have tendency to increase plant stress tolerance by modulating physiological and biochemical processes and further takes part in stimulation of plant growth [28–30]. Molecular docking is also utilized in our present study to demonstrate binding affinity of the synthesized compounds with anticancer proteins and the proteins that aid in plant seed germination [31,32]. Despite extensive research on metal ion sensing, a dedicated system for the highly selective recognition of zirconium(IV) ions remains lacking, particularly one that combines this function with anticancer and antioxidant potential. To address this gap, the present study reports a Schiff base alkyne with indole derivative , demonstrating selective zirconium(IV) ion detection along with promising antiproliferative and antioxidant activities [33]. Lastly, the study explored the compound's ability to promote seed germination.

2. Experimental details

2.1. General information

Indole-3-carboxaldehyde, Propargyl bromide (80 % in toluene) (Sigma Aldrich), Aniline, Potassium Carbonate (98 %, S.D. fine chem. Ltd.), are used in the synthesis process. N, N'-dimethylformamide (DMF, HPLC grade), Methanol, Toluene (Merck) are the organic solvents which were subjected to purification.

The instruments used for mass analysis, UV–visible spectroscopy, chemical shift determination, Thermogravimetric analysis and for performing X-Ray Scattering studies were the same as those detailed in our prior publications [10].

2.2. Synthesis of compound 3

Alkyne was synthesized with the reported procedure from the literature [26]. Firstly indole-3-carboxaldehyde was mixed with potassium carbonate and DMF in a flask. The mixture was stirred over a period of 30 min, then propargyl bromide was added. Then the resultant mixture was stirred again for 18 h at room temperature. After that, the mixture was poured into ice cold water, which caused cream-colored precipitate to form. The solid particles were then separated from the liquid by filter paper and the product 3 was collected. The yield of the reaction was 89 %.

2.3. Synthetic route for Schiff base

For the synthesizing Schiff base, the alkyne 3 and aniline were mixed in equimolar ratio (1:1) in a round bottomed flask and refluxed for 6 h in toluene. Then after the reaction gets over, remaining toluene is evaporated to get crystals of the compound. The synthetic scheme for compound 5 is illustrated in Scheme 1.

2.4. Characterization of Schiff base (E)-N-phenyl-1-(1-(prop-2-yn-1-yl)-1H-indol-3-yl)methanimine (5)

Colour: brown, yield, 89 %, Melting Point: 90–93 °C. ^{1}H NMR (500 MHz, $CDCl_3$) δ 8.63 (s, 1H, -CH═*N*), 8.49 (dd, *J* = 1.4, 0.7 Hz, 1H, N—CH), 7.71–7.18 (m, 9H, Ar-H), 4.91 (s, 2H, ≡C—CH_2), 2.48 (d, *J* = 2.6 Hz, 1H, ≡C—H). ^{13}C NMR (126 MHz, $CDCl_3$) δ 153.05, 152.40, 135.85, 131.56, 128.26, 128.03, 125.32, 123.88, 122.59, 121.55, 121.03, 119.88, 114.86, 114.07, 108.52, 76.20, 75.63, 73.67, 35.25, 1.02. ESI-TOF-MS (ES^+) calculated for $C_{18}H_{14}N_2$: 258.12 Found: 258.09. FT-IR (neat, cm^{-1}): 1616 (ν *C* = *N*), 2129 (ν C≡C), 3270 (ν ≡CH).

2.5. UV–Visible spectral studies

UV-visible spectroscopy was utilized to examine the selectivity and sensitivity of synthesized Schiff base with various metal ions such as Mn^{2+}, Ni^{2+}, Ba^{2+}, Co^{2+}, Cd^{2+}, Cu^{2+}, K^{+}, Pb^{2+}, Rb^{+}, Sn^{2+}, Zn^{2+}, Zr^{4+}. UV-visible spectra were recorded for 10^{-1} M solutions of metal ions in methanol. For the determination of selectivity of 5 for different metal ions, 10 μL of each metal stock solution was used. A significant change in the absorption spectrum was observed for Zr (IV) in comparison with other metal ions. For the ultraviolent titrations, solution of Zr(IV) [10^{-4} M] was gradually added to a stock solution of compound 5. The k_a (association constant) and LOD were then calculated using Benesi-Hildebrand (B-H) plot and a linear calibration curve respectively.

2.6. Growth bioassay

2.6.1. Root length

In this experiment, *Cajanus Cajan* seeds were decontaminated using a 0.1 % sodium hypochlorite solution. Further the seeds were immeresed in solutions of Schiff base with varying concentrations in milligrams per litre viz. 2.5, 5, 7.5 and 10. Then three replicates of each concentration were made, using eight seeds in each patri dish. A Whatman filter paper and a thin layer of damp cotton were placed in each 14 cm diameter petri dish. Each petri dish was then filled with 10 mL of a solution that contained water and DMSO in a ratio of [98:2], with distilled water and DMSO serving as control. The petri dishes were kept in an undisturbed chamber at 20/ 25 °C day and night. The seedlings were gathered after seven days, and a ruler was used to measure the lengths of roots and shoots. The fresh samples of roots and shoots were subsequently dried for 72 h at 60 °C in an oven, and the weights of dried samples were recorded.

2.6.2. Estimation of chlorophyll and protein

Using the technique described by Hiscox and Israesltam (1979), 12 mg of leaves from Cajanus Cajan were extracted for chlorophyll in 2 mL of DMSO. After one-hour incubation at 70 °C, the concentration of solutions was measured spectrophotometrically. Measurements were taken at three wavelengths: 645 nm, 663 nm and 470 nm. The Arnon (1949) equation was used to calculate chlorophyll concentration, which was then expressed on a dry weight basis following the method of Rani and Kohli (1991).

2.6.3. Statistical analysis

The statistical assessment was carried out and the treatment means were compared according to established protocol outlined in relevant literature [10].

2.7. Anticancer study

To evaluate anticancer potential of compound 5, HeLa cells

(obtained from NCCS Pune, India) were exposed to it following a protocol detailed in procedure published in literature [14]. These cells were cultured RPMI medium enriched with 10 % fetal bovine serum (FBS) and 1 % penicillin-streptomycin. The culture environment was maintained at 37 °C under a 5 % CO_2 atmosphere with 95 % humidity. Compound 5 was prepared as 2 mM stock solution in DMSO. For the MTT cell viability assay, 10,000 cells were seeded into each well of 96-well plates. Following a 24 h adjustment period, cells were treated for 48 h with 50 Mm of the synthesized compound, with each condition tested in triplicate. Subsequent to compound treatment, each well received 5mg/ml of MTT solution and was incubated for an additional 3 h at 37 °C. The purple formazan crystals were then dissolved in 200 μL of DMSO, and absorbance was measured at 570 nm using a microplate reader. Paclitaxel (10 nM) served as the positive control. Each experiment was conducted twice to assess cell viability relative to untreated controls [34].

2.8. Antioxidant assay

The DPPH radical scavenging assay was employed to determine the antioxidant activity of compound5. This method is widely accepted for screening the antioxidant potential of chemical compounds due to its rapid execution and reliable accuracy. The assay is based on the hydrogen-donating ability of the antioxidant, wherein the chromogenic radical (DPPH) directly reacts with the compound 5. The change in color intensity was measured spectrophotometrically using UV–Vis spectroscopy, as the absorbance is easily recorded at 517 nm. Different concentrations of the compound 5 and ascorbic acid (12.5, 25, 50, 100, and 200 μg/mL) were prepared in ethanol, and an equal volume of ethanolic DPPH solution was added to each. The mixtures were incubated for 30 min at room temperature in the dark. The decrease in DPPH absorbance at 517 nm was recorded, indicating the extent of radical scavenging. Ascorbic acid was used as a reference standard under the same conditions [35].

2.9. X-Ray diffraction studies

Once the reflux was finished, compound 5 crystals were produced by evaporating the toluene. The crystal was prepared for analysis by being mounted on a polarizing microscope with the aid of Hampton CryoLoop. A Super-Nova (Mo) X-ray diffractometer with a microfocus sealed X-ray tube equipped with Mo-Ka radiation at $\lambda = 0.71073$ Å as an X-ray source and a HyPix3000 (CCD plate) detector that scans at a rate of 5 to 10 s/frame, with a width that increases by 0.3 per frame was used to gather the single crystal data. The SHELXL refinement package and Olex2 with ShelXT structure solution program were used to solve and refine the structure, respectively. Intrinsic phasing was used for the structure solution, while least squares minimization was used for the refinement. Mercury 4.0.0 software uses a variety of techniques and parameters to draw the crystal structure. The CCDC number for the crystal of compound 5 is 2388,270.

2.10. Molecular docking protocols

To gain deeper insights into the interaction mechanisms between the synthesized ligands and target proteins, molecular docking simulations were performed using AutoDock 4.2.6 coupled with AutoDock Tools 1.5.7 [36]. The 3D crystal structures of the anticancerous protein and gibberellin protein with PDB Id: 4xr8 and 4psb respectively were retrieved from the Protein Data Bank (PDB), while the ligand molecule IK was designed and energy-minimized prior to docking. The initial 2D ligand structures were generated using ChemDraw and subsequently converted into 3D conformers. Geometry optimization was carried out in Avogadro Molecular Editor using the MMFF94 force field, ensuring stable, low-energy conformations suitable for docking. The optimized ligand structures were saved in PDBQT format for compatibility with AutoDock. Protein structures were preprocessed in AutoDock Tools 1.5.7, which involved removing bound water molecules and non-essential heteroatoms, addition of polar hydrogens, and assignment of Kollman charges to improve docking accuracy. The grid dimensions for 4xr8 were established as x=−26.763, y=−28.107, z=−12.111 and the same for 4psb were $x = 0.181$, y= −1.266, $z = 17.489$. The docking grid box was defined around the active site with dimensions of 60 × 60 × 60 points and a spacing of 0.375 Å, centered on the binding pocket to maximize the probability of ligand–receptor interactions. Docking simulations were executed using the Lamarckian Genetic Algorithm (LGA) with 100 independent runs, a population size of 150, a maximum of 2.5 × 10^6 energy evaluations, and 27,000 generations, ensuring comprehensive exploration of potential binding conformations. To validate the docking protocol, the native co-crystallized ligand of each receptor was re-docked into its binding site, and the RMSD values between the docked and crystallographic poses were calculated. RMSD values below 2.0 Å confirmed the reliability and accuracy of the docking setup. The docking results were evaluated based on the lowest binding energy poses and corresponding interaction patterns, which revealed the most favourable binding modes of each ligand with the receptor proteins. Visualization and interaction analyses were carried out using Accelrys Discovery Studio Visualizer 4.0, AutoDock Tools, and Protein Plus, providing detailed insights into hydrogen bonding, hydrophobic interactions, and π–π stacking between the ligands and active site residues. This integrative docking workflow, validated and parameterized for reproducibility, enabled a systematic evaluation of ligand–protein interactions, thereby complementing the experimental findings and highlighting the potential of indole-based Schiff base ligands as promising candidates for bioactive applications.

2.11. Synthesis of metal complex

Equivalent amounts of metal and the ligand were mixed together in a round bottomed flask taking methanol as the solvent for synthesizing metal-ligand complex. After stirring the reaction mixture for 4 h, the solvent was allowed to evaporate. Through the use of DFT, IR spectroscopy, NMR spectroscopy and mass spectrometry, a brown metal-ligand formation was confirmed.

2.12. DFT calculations

DFT calculations using Gaussian 09 software were performed for structure optimization of 5 and its Zr(IV) complex. To obtain the optimized structure of 5, B3LYP/6–311 G level of theory was used. On similar basis, LAN2DZ was bought into service for energy minimization of complex. The HOMO and LUMO energies were computed.

2.13. Pharmakokinetic prediction

Rather than relying on lengthy and uncertain therapeutic testing, the development of new drugs can be significantly expedited by assessing their physiochemical properties. Online resources like PreADMET

Table 1
Predicted physiochemical properties of synthesized compound 5 based on Lipinski's rule.

Compound	M.W.	TPSA	M_i Log P	N Rot B	n-ON acceptor	n-OHNH donar	Lipinski violations
Rule	<500	<70	<5	<15	≤10	≤5	≤1
5	258.32	17.30	3.85	3	2	0	0

Table 2
Pharmacokinetic prediction of compound 5.

Compound	BBB	Caco-2 cell permeability (nms^{-1})	Plasma Protein Binding (%)	MDCK (nms^{-1})	HIA	Skin permeability (log Kp)
5	1.87027	26.4072	91.480285	13.9942	100	−1.81995

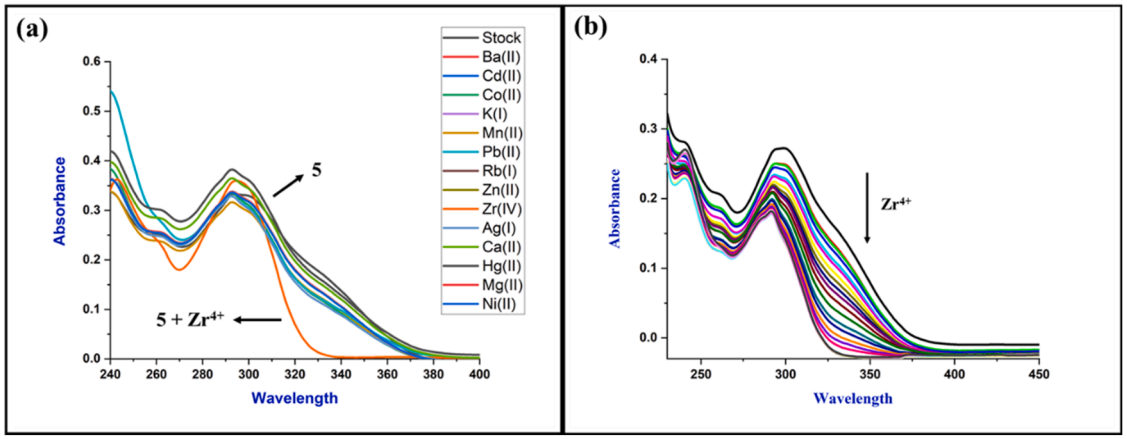

Fig. 1. (a) UV-visible absorbance spectra of 5 along with various metal ion. (b) UV-visible Titration plot of 5 with Zr(IV).

(http://preadmet.bmdrc.org) and Molinspiration (http://molinspiration.com) provide valuable insights into these crucial characteristics. For a compound to be considered orally accessible, it must satisfy specific criteria: a molecular weight of 500 or less, an m_i log P of 5 or less, a topological polar surface area (TPSA) of 70 or less, a maximum of 10 hydrogen bond acceptors, no >5 hydrogen bond donors, and a limit of 15 rotatable bonds. These parameters offer predictive information, with rotatable bonds indicating adaptability, m_i log P reflecting hydrophilicity, and TPSA suggesting drug absorption. The physiochemical profile of compound 5, as determined by these tools, is presented in Table 1.

Online predictive models for ADMET (Absorption, Distribution, Metabolism, Excretion, and Toxicity) provide crucial pharmacokinetic data for new compound. These models quantify parameters such as plasma protein binding (PP Binding), which influences drug disposition and therapeutic efficacy. Data from the Caco-2 cell line and assessments of human intestinal absorption (HIA) are directly relevant to evaluating oral bioavailability and transdermal penetration into the systemic circulation. Furthermore, blood-brain barrier (BBB) penetration assays are indispensable for determining a drug's accessibility to the central nervous system. Additional ADMET parameters include Madin-Darby Canine Kidney (MDCK) assays and skin permeability measurements. The collective ADMET profiles of the synthesized compound, as presented in Table 2, provide compelling evidence for their therapeutic potential [37,38].

3. Results and discussion

3.1. Synthesis and characterization

As depicted in Scheme 1, the synthetic route was followed in order to synthesize compound 5 commenced by synthesis of alkyne 3. Indole-3-carboxaldehyde and potassium carbonate (K_2CO_3) were added to 100 mL round- bottom flask containing DMF solvent, followed by the addition of propargyl bromide after 30 min of stirring. After 18 h of stirring, it was added to ice cold water and allowed to work up. The product was subsequently filtered and collected. Compound 3 was used for further synthesis of product 5. After reacting with aniline in a toluene solvent, it was refluxed for 6 h at 110 °C. Then toluene was evaporated yielding crystals of compound 5. Single crystal XRD, Mass spectrometry and NMR (^1H and ^{13}C) verifies the molecular structure of 5.

3.2. UV–Visible study

3.2.1. UV–Visible spectral analysis

Methanol was used as the base solvent for the metal detecting process, and the concentration of the compound was set at 6×10^{-6} mol L^{-1}. A significant change was shown in case of Zirconium after adding 10 μL of several metal ions including Ba^{2+}, Cd^{2+}, Co^{2+}, Cu^{2+}, K^{+}, Mn^{2+}, Pb^{2+}, Ni^{2+}, Rb^{1+}, Sn^{2+}, Zn^{2+} and Zr^{4+}, to compound 5 and is shown in Fig. 1 (a).

3.2.2. Titration study

The responsiveness of compound 5 to Zr (IV) was evaluated via titration. The experiment involved gradual addition of 10^{-4} M solution of Zirconium (IV) to a solution of compound 5 having concentration 6×10^{-6}M This causes a reduction in the absorption band at 330 nm (hypochromic shift). The limit of detection was determined to be 370 nM (Fig. 3(a)). This calculation was based on the formula 3/s, where sigma is standard deviation and s is the slope of calibration curve. The titration plot is shown in Fig. 1(b).

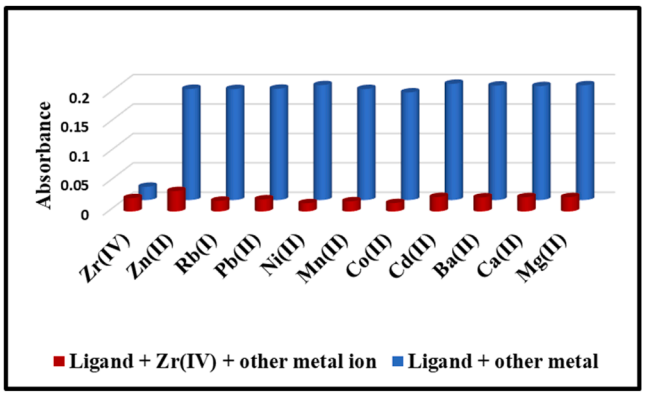

Fig. 2. Metal interference study.

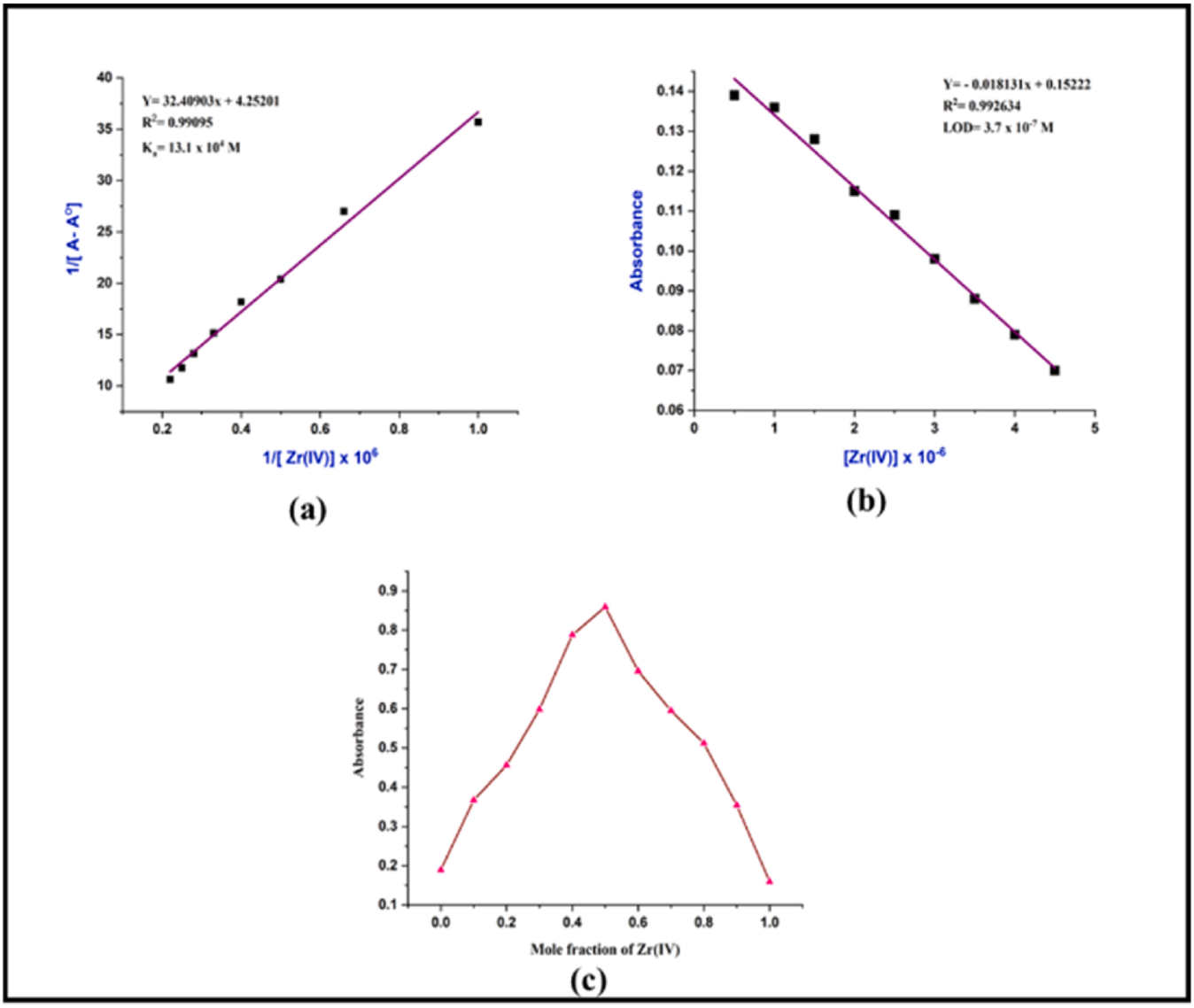

Fig. 3. (a) B-H Plot (b) LOD Plot (c) JOB's Plot.

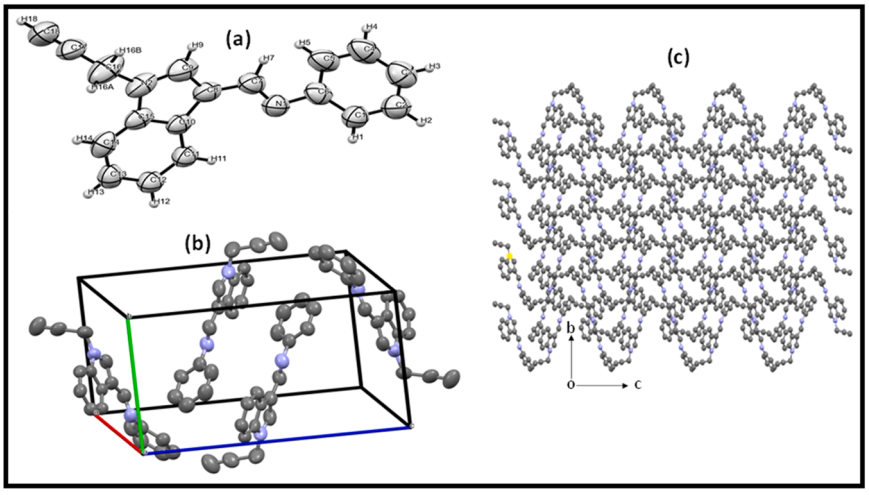

Fig. 4. (a) ORTEP diagram of compound 5. (b) Monoclinic unit cell of compound 5. (c) 2D sheet like structure of compound 5.

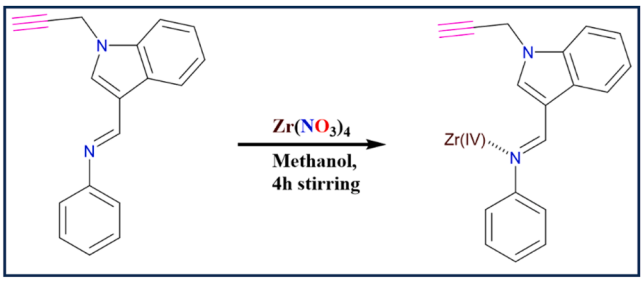

Scheme 2. Synthesis of metal complex.

3.2.3. *Metal interference study*

The potential for other metal ions to affect the detection of Zr(IV) by 5 was investigated through an interference study. Equivalent concentrations of Zn(II), Pb(II), Rb(I), Ni(II), Co(II), Mn(II), Cd(II), Ba(II), Ca(II) and Mg(II) were individually introduced to a solution of compound 5 pretreated with Zr(IV) in methanol. The resulting solutions were subjected to spectrophotometric analysis and the plot is shown in Fig. 2.

3.2.4. *Stoichiometric complexation ratio*

Equimolar concentrations of the ligand and metal were used to create the job's plot in order to determine the stoichiometric ratio between them. The job's plot shows the highest point at 0.5, which confirms that the ligand and the metal binds together in a ratio of 1:1 as shown in Fig. 3(c).

3.3. *Thermogravimetric analysis*

TGA, a useful method for calculating weight loss in relation to temperature, was used to examine the thermal stabilities of the Schiff base. Under a nitrogen environment, the analysis was conducted between 25 °C and 1000 °C in temperature.

Compound 5 exhibits two distinct phases of decomposition. The first stage involves a weight loss from 70 °C to 150 °C, primarily caused by moisture. Since no appreciable weight loss was seen until 250 °C, compound 5 is therefore stable till 250 °C. Since TGA curve for Schiff base curve shows no distinct weight loss up to 250 °C is one characteristic of thermally stable compounds. (Fig. S7)

3.4. *Crystallographic analysis*

Using X-ray crystallography, the crystal structure of compound 5 which has the chemical formula $C_{18}H_{14}N_2$, was determined to be monoclinic in shape in space group $P2_1/n$. The ORTEP diagram for crystal representation of compound 5 is shown in the Fig. 4(a). Within the crystal, each unit cell comprises of four molecules. This arrangement reveals structural features and molecular conformations of compound 5 Fig. 4(b). The unit cell has dimensions of $a = 11.5292$ (10) Å, $b = 8.7066$ (7) Å, $c = 14.2477$(10) Å, with angles $\alpha = \gamma = 90°$, $\beta = 97.27$ (7). The volume V of unit cell is 1418.7 (2) Å^3, resulting in the calculated density (ρcalc) of 1.209 g·cm^{-3}. The N1-C7 bond length is 1.271 Å, which is characteristic of ($C = N$) bond. Molecular visualizations were prepared using Mercury version 4.0.0. The packing arrangement of 2D crystal structure, when visualized from a-axis, reveals a chain linked sheets that unfolds along the b and c-axes Fig. 4(c).

3.5. *Mode of binding*

Spectroscopic analyses, including IR spectroscopy and ^{1}H NMR, confirmed the interaction between Zr(IV) and compound 5. In the infrared spectra, a notable shift from 1616 cm^{-1} to 1663 cm^{-1} (Fig. S5)

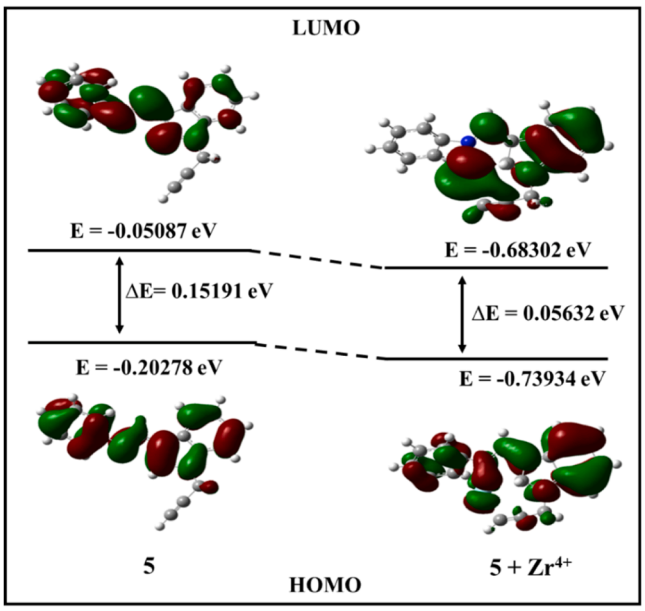

Fig. 5. HOMO and LUMO energy representation for 5 and 5 + Zr^{4+}.

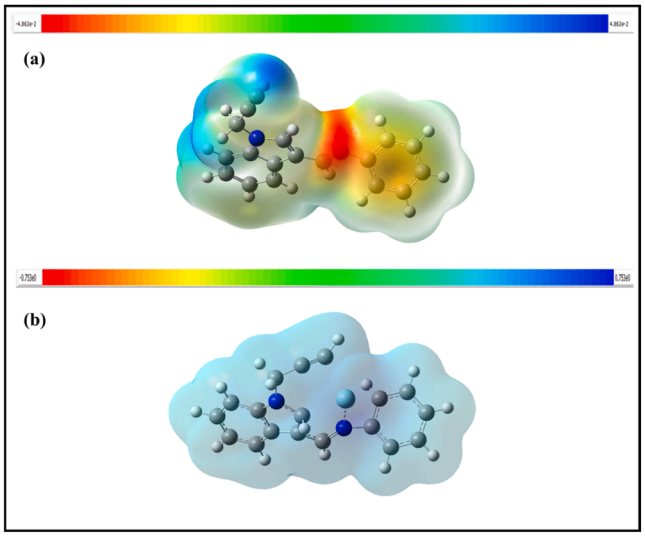

Fig. 6. Molecular Electrostatic potential for (a) Compound 5 (b) Compound 5 complex with Zr(IV).

indicated the presence of an imine group. Similarly, the 1H NMR spectrum showed a chemical shift from 8.63 ppm to 8.84 ppm (Fig. S6) after Zr(IV) interacted with the ligand. These changes strongly suggest that zirconium binds specifically to the imine ($C = N$) moiety of the ligand. Scheme 2 illustrates the synthetic route employed for the synthesis of metal complex.

3.6. *DFT investigation*

The optimization of structure of 5 was done using gaussian 09 software and generated its lowest unoccupied molecular orbital and highest occupied molecular orbital. Subsequently, the energy difference between both orbitals was calculated as 0.152 eV. The energy optimization was obtained using B3LYP/ 6–311 G levels and LAN2DZ basis set.

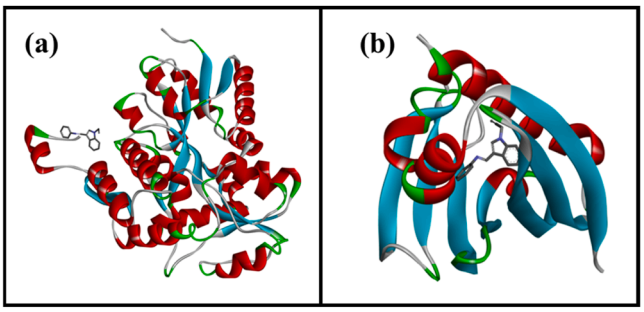

Fig. 7. Representation of compound 5 bound at the active site of protein (a) 4xr8 (b) Gibberellin.

Similarly, after optimizing 5 + Zr complex structure, the HOMO-LUMO energy gap was determined to be 0.056 Ev as shown in Fig. 5.

3.7. Molecular electrostatic potential analysis

Molecular Electrostatic Potential (MEP) analysis was performed to understand the charge distribution and potential reaction sites of our molecule. The MEP maps, calculated with Gaussian software, utilize a color scale where red indicates electron-rich, negative potential; blue signifies electron-deficient, positive potential; and green represents intermediate potential. For compound 5, the MEP map as depicted in Fig. 6(a) shows a wide potential range from -4.862×10^{-2} to 4.862×10^{-2}.

The presence of intense red regions, particularly around electronegative atoms like Nitrogen, confirms their electron-rich nature. This makes these sites highly favorable for interaction with electrophiles, such as the Zirconium(IV) used in this study. The Molecular Electrostatic Potential (MEP) surface of the compound after complexation with Zr(IV) clearly reflects the redistribution of electron density upon binding with a new potential range of −0.753 to 0.753 as shown in Fig. 6(b). In the complex, blue regions appear around the Zr(IV) coordination sites, highlighting strong electron deficiency resulting from the Lewis acidic nature of Zr(IV), which withdraws electron density from the donor atoms of the ligand. This confirms that the nitrogen atoms, which previously exhibited highly negative potential before complexation, have now lost electron density upon coordination, shifting from red toward green or blue zones. Overall, the change in color distribution, especially the appearance of positive blue patches near the metal center, provides strong evidence for successful Zr(IV) binding and illustrates the altered electronic environment of the ligand after complexation [39].

3.8. Molecular docking analysis

The final docked structures, visualized using Discovery Studio 4.0, revealed minimum binding energies of −6.36 Kcal/mol and −7.20 Kcal/

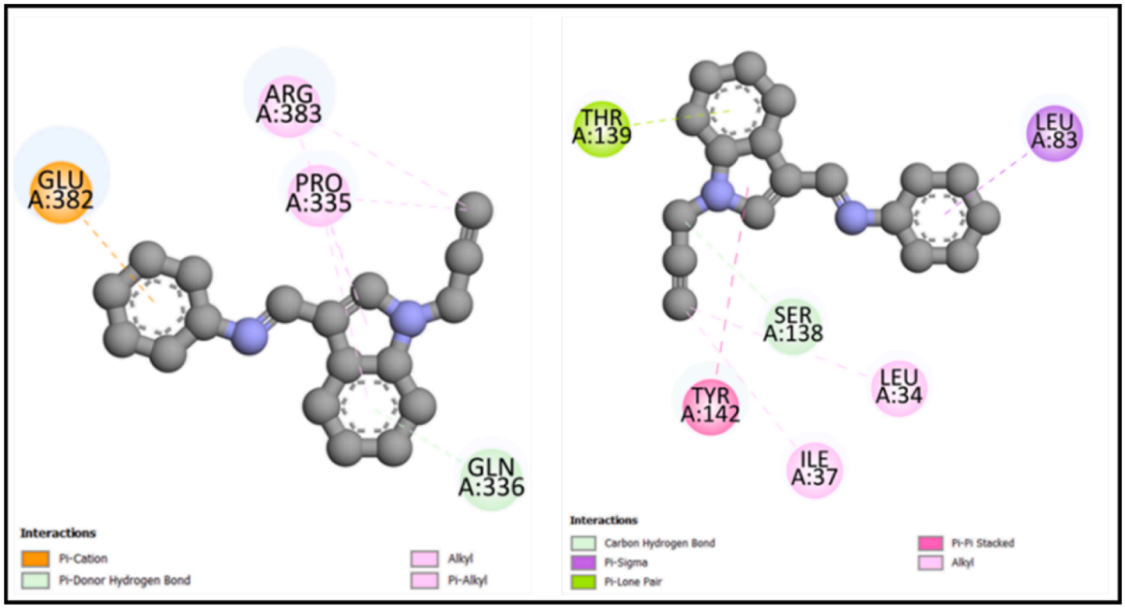

Fig. 8. 2D diagram for protein ligand interaction of 5 with amino acids of protein (a) 4xr8 (b) Gibberellin.

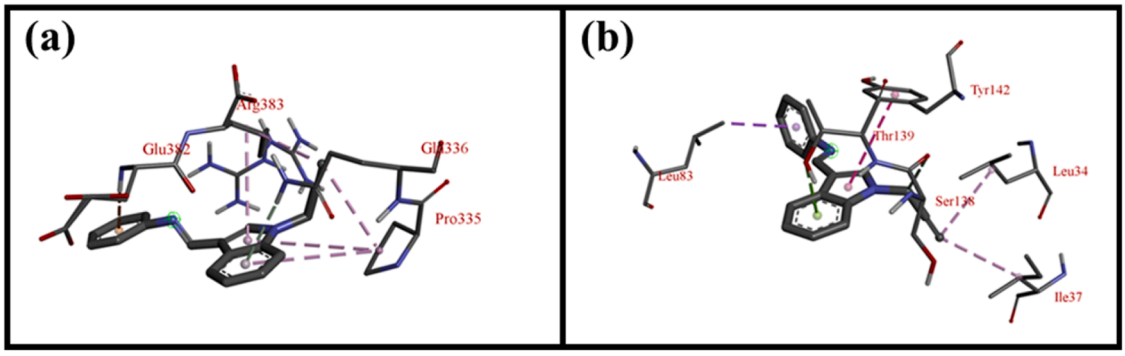

Fig. 9. 3D Docking interaction of compound 5 with active site of (a) 4xr8 (b) Gibberellin.

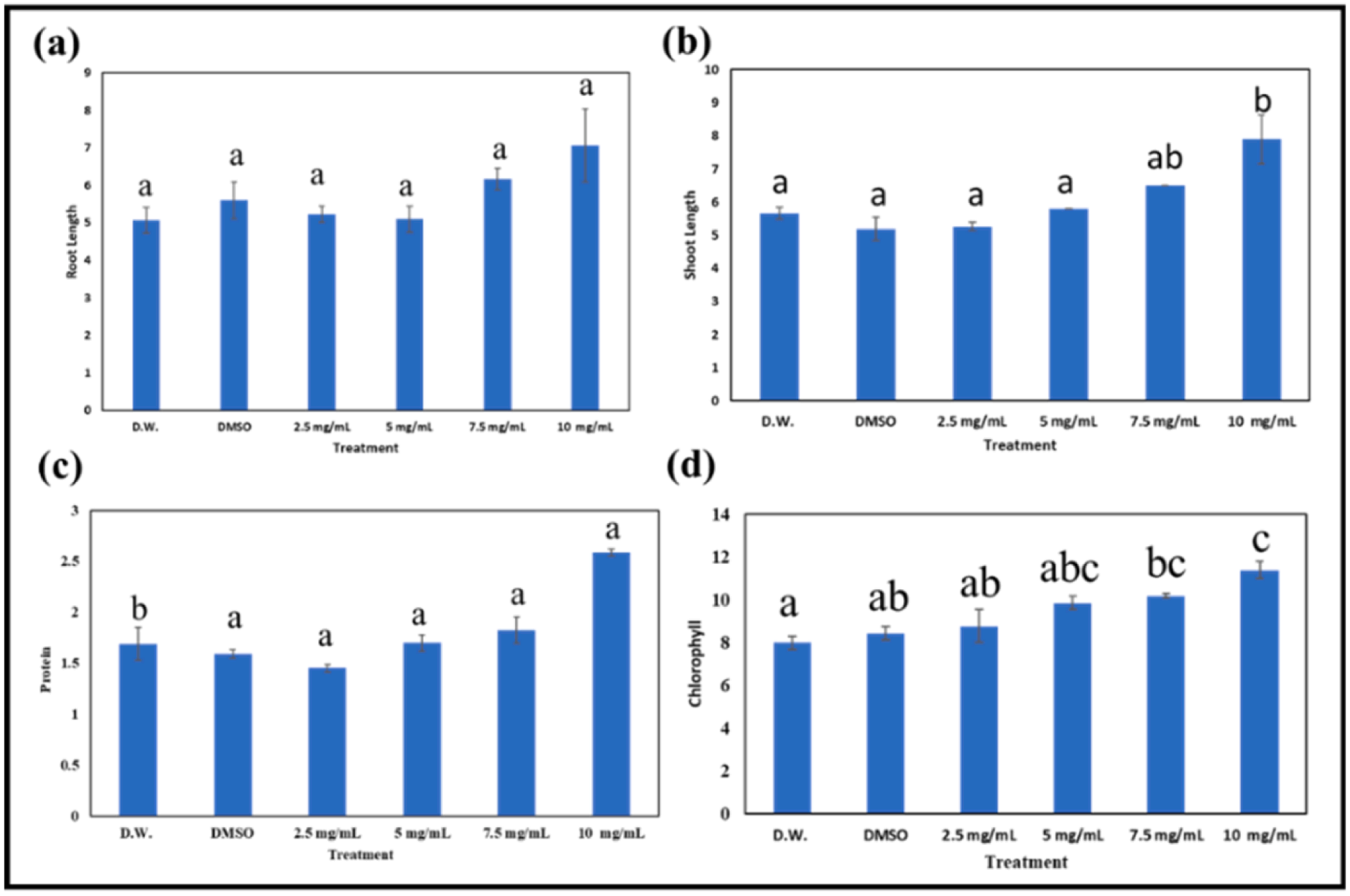

Fig. 10. Effect of 5 on *Cajanus cajan* (a) Root Length (b) Shoot Length (c) Protein (d) Chlorophyll (Here the groups with letters (a), (b) and (c) represents that they are significantly different from each other (typically at $p < 0.05$). The letter (ab) indicates that the group is not significantly different from either (a) or (b), placing it in between the two. Similarly (bc) and (abc) indicates they are not significantly different from either of them and are placed in between the two).

mol for the two proteins, respectively. Fig. 7 illustrates the binding of compound 5 at the active site of protein 4xr8 (a) and Gibberellin (b). Further details on the binding sites and interactions are provided in Fig. 8 which illustrates 2D diagrams of protein-ligand interactions of compound 5 with amino acids of docked proteins, while Fig. 9 displays the 3D docking interactions of compound 5 with the active sites showing hydrophobic and hydrogen bonding interactions. Quantitative data on hydrophobic and hydrogen bonding interactions of compound 5 with the docked proteins are tabulated in Tables S1 and S2.

3.9. Bioassay studies

Compound 5 demonstrably impacts *Cajans cajan* growth. The most substantial growth enhancement reflected in increased shoot length, chlorophyll levels, and protein content, occurred when the plants were exposed to 10 mg/L. The outcomes are depicted in Fig. 10 and Fig. 11.

3.10. Antioxidant activity

The DPPH radical scavenging assay was employed to evaluate the antioxidant capacity of the ligand. The results indicated the presence of donatable hydrogen atoms in the ligand, as evidenced by the color change of the DPPH methanolic solution from violet to yellow upon interaction with the antioxidant. Fig. 12(a) depicts the color changein DPPH solution upon addition of compound 5 and ascorbic acid. The compound exhibited notable antioxidant activity; however, its activity was lower compared to that of ascorbic acid. The antioxidant potential of 5 is enhanced by the presence of functional groups capable of donating electrons or hydrogen atoms. Thus, this study suggests that compound 5 hold promising potential as antioxidant agents. The data further revealed a concentration-dependent increase in the free radical scavenging activity of the compound, indicating its ability to neutralize more radicals at higher concentrations. (Fig. 12(b))

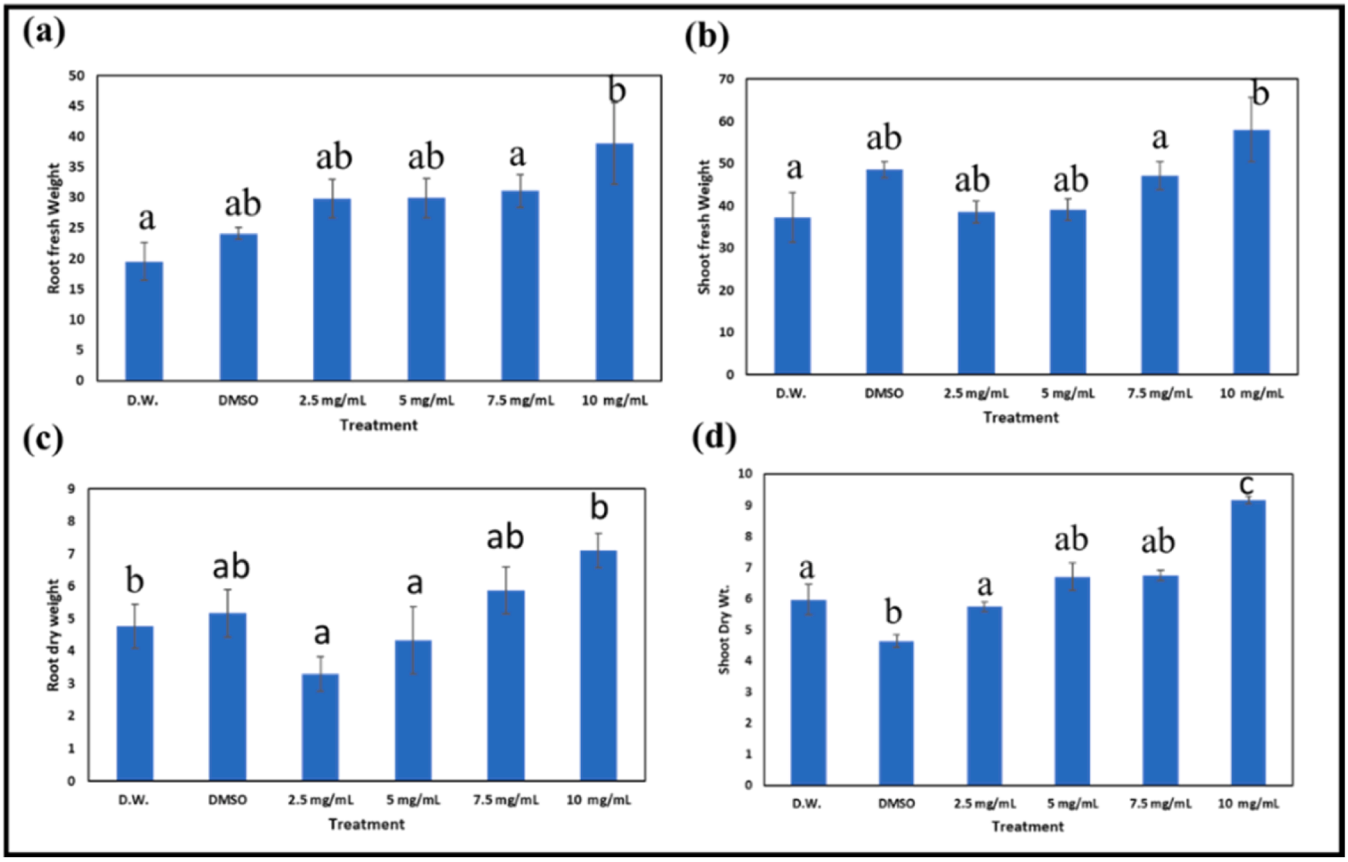

Fig. 11. Effect of 5 on *Cajanus cajan* (a) Root fresh weight (b) Shoot fresh Weight (c) Root dry weight (d) Shoot dry weight (Here the groups with letters (a), (b) and (c) represents that they are significantly different from each other (typically at $p < 0.05$). The letter (ab) indicates that the group is not significantly different from either (a) or (b), placing it in between the two).

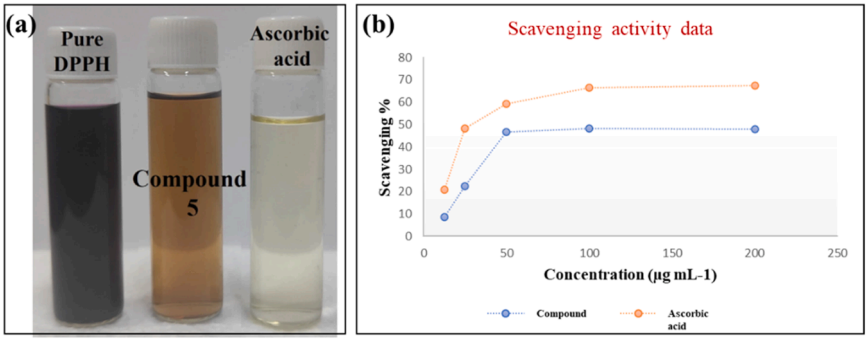

Fig. 12. (a) Colour change in DPPH solution on the addition of ascorbic acid and compound 5 (b) Scavenging activity of 5 with ascorbic acid.

3.11. Anticancer activity

The anticancer properties of compound 5 was explored through a 24 h exposure of HeLa cervical cancer cells. The significant MTT assay demonstrated that compound 5 significantly decreases Hela cell viability to 67.67 % which indicates its prominent efficacy. Fig. 13(a) represents the % cell viability of 5 w.r.t. control cell after the treatment with cancer cells. Furthermore, dose response curve for compound 5 (Fig. 13(b)) illustrates the relationship between compound concentration and cell viability. With increase in the concentration of compound 5, there is a corresponding decrease in the percentage of viable cells, indicating a dose-dependent cytotoxic effect. At lower concentrations, the compound shows minimal impact on cell viability, whereas at higher concentrations, a significant reduction in cell viability is observed. This pattern suggests that compound 5 exerts its biological activity in a concentration-dependent manner, with potential implications for its use as an anticancer or cytotoxic agent.

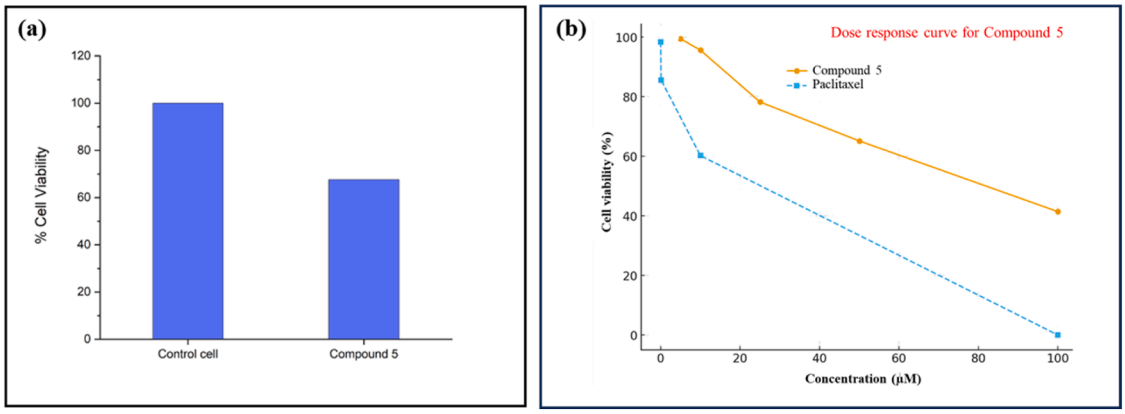

Fig. 13. (a) %age Cell Viability of 5 (b) Dose response curve for 5.

4. Conclusion

In this work reported herein, the Schiff base is effectively derived and thoroughly characterized utilising ^{1}H NMR, ^{13}C NMR, UV spectroscopy, IR spectroscopy, Mass spectrometry and SCXRD. It validates a strong potential for detection of Zirconium(IV). Analysis by UV spectrophotometry depicted a good detection limit and strong association constant of 3.7×10^{-7} M and 13.1×10^{4} M respectively. The Job's plot analysis depicted a 1:1 binding ratio with Zirconium(IV) and 5. The proposed binding mode was further supported by DFT calculations and spectroscopic characterization of the synthesized zirconium-ligand complex. Beyond its other application, the synthesized probe 5 has shown promise as an anticancer agent which was strengthened by molecular docking studies with the target protein. Moreover, its ability to promote seed germination opens up possibilities for agricultural application.

Associated content

The supporting information contains ^{1}H NMR, ^{13}C NMR, FTIR and Mass Spectrometry data along with TGA Curve and possible interactions with docked proteins.

Data availability

The data that supports the findings of this study are available in the supplementary material of this article.

CRediT authorship contribution statement

Gurjaspreet Singh: Writing – review & editing, Visualization, Validation, Supervision, Project administration, Funding acquisition, Conceptualization. **Parul:** Writing – original draft, Investigation, Conceptualization. **Ankush Sheoran:** Resources. **Baljinder Singh Gill:** Conceptualization. **Deepanjali Baliyan:** Formal analysis. **Amarjit Kaur:** Supervision. **Daizy Rani Batish:** Formal analysis. **Aditi Rana:** Formal analysis. **Brij Mohan:** Resources.

Declaration of competing interest

The authors declare that they have no known competing financial interests or personal relationships that could have appeared to influence the work reported in this paper.

Acknowledgement

The authors are thankful to University Grant Commission (UGC), DST-FIST-0215 (SR/FST/CS11–36) and RUSA 2.0 for providing financial support.

Supplementary materials

Supplementary material associated with this article can be found, in the online version, at doi:10.1016/j.molstruc.2025.144049.

References

[1] A.K. Chitoria, A. Mir, M.A. Shah, A review of ZrO2 nanoparticles applications and recent advancements, Ceram. Int. 49 (2023) 32343–32358.
[2] W. Shen, G. Wang, S. Wang, Y. Zhang, J. Kang, Z. Xiao, X. Fu, Designing and vat photopolymerization 3D printing of glass ceramic/zirconia composites functionally gradient ceramics for dental restorations, Ceram. Int. 51 (2025) 4441–4452.
[3] D.K. Gupta, S. Kumar, M.Y. Wani, MOF magic: zirconium-based frameworks in theranostic and bio-imaging applications, J. Mater. Chem. B 12 (2024) 2691–2710.
[4] B. Basnet, R. Huang, B.T. Tabatabaei, J.W. Choi, Additive manufacturing of binder-coated zirconia on a freeform surface, J. Eur. Ceram. Soc. 45 (2025) 117127.
[5] S. Sampurnam, S. Muthamizh, A. Khusro, K.A. Varman, V. Narayanan, In vitro assessment on antibacterial, antioxidant, and anticancer traits of chemically synthesized polyaniline/ZrO2-Ag nanohybrid, Bionanoscience 15 (2025) 1–11.
[6] S. Preetha, P. Anilkumar, N. Jenifar A, Comparative investigation of structural properties and biological applications of chemical and biogenic synthesis of zirconium dioxide (ZrO2) nanoparticles using Passiflora edulis, J. Photochem. Photobiol. B: Biol. 263 (2025) 113089.
[7] G. Singh, P. Malik, Mohit Pawan, A. Devi, S. Gupta, A. Singh, K.N. Singh, Azomethine functionalized platform for the selective detection of Zr (IV) ion, biological evaluation and potent TLR-4 inhibitor, J. Mol. Struct. 1297 (2024) 136916.
[8] T. Xu, W. Wang, Effect of filling strategy on surface topography and strength of 3D–printed dense zirconia ceramics, Ceram. Int. (2025).
[9] L.Z. Kang, Y.H. Lu, W.W. Bian, P.J. Yu, Y.B. Wang, L. Xin, Y.M. Han, Fretting corrosion behavior and microstructure evolution of hydrided zirconium alloy under gross slip regime in high temperature high pressure water environment, Corros. Sci. 242 (2025) 112582.
[10] G. Singh, S. Khurana, Mohit Pawan, A. Devi, A. Singh, Vikas, D.R. Batish, A. Sharma, A piperazine-modified Schiff base sensor for highly selective detection of Zr (IV) ions: unveiling its antioxidant potential and regulatory effects on zea mays growth, Int. J. Biol. Macromol. 261 (2024) 129689.
[11] S. Kiechle, A. Liebermann, G. Mast, M. Heitzer, S.C. Möhlhenrich, F. Hölzle, H. Kniha, K. Kniha, Evaluation of one-piece zirconia dental implants: an 8-year follow-up study, Clin. Oral Investig. 27 (2023) 3415–3421.
[12] P. Gao, Q. Zhang, Y. Sun, H. Cheng, S. Wu, Y. Zhang, W. Si, H. Sun, N. Sun, J. Yang, K. Cai, Lei Lu, J. Liu, Synergistic catecholamine and coordination chemistry for enhanced bioactivity and secondary grafting activity of zirconia dental implants, Colloids. Surf. B Biointerfaces. 246 (2025) 114361.
[13] G. Singh, Y. Thakur, Heena Mithun, S. Sharma, H. Kaur, C. Espinosa-Ruíz, M. A. Esteban, K.N. Singh, Synthesis of Schiff base functionalized organosilatranes for the detection of zirconium (IV) ion: their cytotoxicity evaluation and anti-inflammatory activity against cyclooxygenase-2 via computational approach, Appl. Organomet. Chem. 38 (2024) 7297.
[14] G. Singh, S.Khurana Heena, B.S.Gill Mithun, D. Baliyan, Vikas, N. Dege, E. Tarcan, Pseudoagostic interaction based zirconium sensing using 1, 2, 3-triazole and its anticarcinogenic potential evaluation through In Vitro and In Silico approach, Appl. Organomet. Chem. 39 (2025) 7983.
[15] A.O. Keikha, S. Shahraki, E. Dehghanian, H. Mansouri-Torshizi, Effect of central metal ion on some pharmacological properties of new Schiff base complexes. Anticancer, antioxidant, kinetic/thermodynamic and computational studies, Spectrochim. Acta a Mol. Biomol. Spectrosc. 325 (2025) 125034.
[16] Y.M. Ahmed, M.A. Elgendi, M.M. Omar, G.G. Mohamed, R.G. Deghadi, Synthesis, characterization, antimicrobial, antioxidant studies, molecular docking and DFT calculations of novel Schiff base and its metal complexes, J. Mol. Struct. 1326 (2025) 141076.

[17] K.M. Tawfiq, H.A.S. Al Naymi, S.M. Obaid, T.H. Al-Noor, A.J. Al-Sarray, Synthesis, characterization, molecular docking, cytotoxicity, and antimicrobial activity of schiff base Ligand and its metal complexes, Appl. Organomet. Chem. 39 (2025) 7781.
[18] S.S. Ibrahim, M.Y. Al-darwesh, S.W. Arkawazi, K.A. Babakr, I.N. Qader, Synthesis, characterization, antioxidant, antibacterial activity, and molecular docking studies of Zn (II) and Cu (II) complexes nanoparticles, J. Mol. Struct. 1326 (2025) 141120.
[19] H. Luesch, E.K. Ellis, Q.Y. Chen, R. Ratnayake, Progress in the discovery and development of anticancer agents from marine cyanobacteria, Nat. Prod. Rep. (2025).
[20] F.Khan Zainab, A. Alam, N.U. Rehman, S. Ullah, A.A. Elhenawy, M. Ali, M.U. Islam, A. Khan, A. Al-Harrasi, M. Ahmad, Y. Haitao, Synthesis, anticancer, α-glucosidase inhibition, molecular docking and dynamics studies of hydrazone-Schiff bases bearing polyhydroquinoline scaffold: in vitro and in silico approaches, J. Mol. Struct. 1321 (2025) 139699.
[21] E.R. Kenawy, H. Tenhu, M.M. Azaam, S.A. Khattab, M.E. Kenawy, A.M. Radwan, H. A. Abosharaf, Schiff bases of cellulose: synthesis, characterization, and anticancer potency against hepatocellular carcinoma, Int. J. Biol. Macromol. (2025) 140506.
[22] M. Jiang, X. Su, X. Zhong, Y. Lan, F. Yang, Y. Qin, C. Jiang, Recent development of Schiff-base metal complexes as therapeutic agents for lung cancer, J. Mol. Struct. (2024) 139403.
[23] E. Milović, J.T. Ristovski, S. Stefanović, J. Petronijević, N. Joksimović, I.Z. Matić, A. Đurić, B. Ilić, O. Klisurić, M. Radan, K. Nikolić, Synthesis, in vitro anticancer activity, and pharmacokinetic profiling of the new tetrahydropyrimidines: part I, Arch. Pharm 357 (2024) 2400403.
[24] L. Lv, T. Zheng, L. Tang, Z. Wang, W. Liu, Recent advances of Schiff base metal complexes as potential anticancer agents, Coord. Chem. Rev. 525 (2025) 216327.
[25] S.S. Marufa, M.M. Rahman, M.M. Rahman, J.R. Debnath, M.A. Mim, R. Jahan, H. Nishino, M.S. Alam, M.A. Haque, Conventional and microwave-assisted synthesis, antimicrobial and antioxidant activity evaluation with in silico studies of carbazole-thiazole-Schiff base hybrids, J. Mol. Struct. 1321 (2025) 139861.
[26] G. Singh, Y. Thakur, A. Saini, A. Devi, S.Khurana Tamana, K.N. Singh, D.R. Batish, A. Sharma, Synthesis of modified Schiff base triazole appended silatrane: elucidating the in vitro and in silico plant growth potential, J. Mol. Struct. 1312 (2024) 138455.
[27] Y. Guo, J. Wang, W. Liu, J. Liu, C. Wang, Q. Wu, Z. Wang, Construction of magnetic hydroxyl group-enriched hyper cross-linked polymers with functional triazine as the core for efficient enrichment of plant growth regulators, Food Chem. 433 (2024) 137309.
[28] Z. Chen, Q. Liu, S. Zhang, Y. Hamid, J. Lian, X. Huang, T. Zou, Q. Lin, Y. Feng, Z. He, X. Yang, Foliar application of plant growth regulators for enhancing heavy metal phytoextraction efficiency by Sedum alfredii Hance in contaminated soils: lab to field experiments, Sci. Total. Environ. 913 (2024) 169788.
[29] F.U. Haider, Noor-ul- Ain I. Khan, M. Farooq, L.Cai Habiba, Y. Li, Co-application of biochar and plant growth regulators improves maize growth and decreases Cd accumulation in cadmium-contaminated soil, J. Clean. Prod. 440 (2024) 140515.
[30] S. Jan, R. Bhardwaj, N.R. Sharma, R. Singh, Unraveling the role of plant growth regulators and plant growth promoting rhizobacteria in phytoremediation, J. Plant Growth Regul. (2024) 1–17.
[31] P. Xie, X. Wang, Y. Deng, C. Zhang, Y. Zhang, L. Huang, Deciphering non-covalent binding mechanism of olive biophenolic secoiridoids interaction with β-lactoglobulin: multi-spectroscopies, thermodynamics, molecular docking, and molecular dynamics simulation, Food Hydrocoll. 162 (2025) 110897.
[32] H.S. Seleem, G.A. El-Inany, H.F. El-Shafiy, B.A. El-Shetary, F.I. Hanafy, A.I. Nabeel, A. Madyan, M. Shebl, Unveiling the coordinating manner of a novel quinoline-based hydrazone towards Co (II), Ni (II) and Cu (II) ions: synthesis, physicochemical, DFT, anticancer and molecular docking studies, J. Mol. Struct. (2025) 141458.
[33] M. Fallah-Mehrjardi, H. Kargar, K.S. Munawar, Tridentate ONO hydrazone Schiff base complexes in organic transformations: catalytic and mechanistic studies, Inorganica Chim. Acta 560 (2024) 121835.
[34] X. Lin, T. Yu, L. Zhang, S. Chen, X. Chen, Y. Liao, D. Long, F. Shen, Silencing Op18/stathmin by RNA interference promotes the sensitivity of nasopharyngeal carcinoma cells to taxol and high-grade differentiation of xenografted tumours in nude mice, Basic Clin. Pharmacol. Toxicol. 119 (2016) 611–620.
[35] W. Brand-Williams, M.E. Cuvelier, C.L.W.T. Berset, Use of a free radical method to evaluate antioxidant activity, LWT-Food Sci. Technol. 28 (1) (1995) 25–30.
[36] S.K. Ramadan, W.S. Abou-Elmagd, E.M. Hosni, M. Kamal, A.I. Hashem, E.A. El-Helw, Synthesis, in vivo evaluation, and in silico molecular docking of benzo [h] quinoline derivatives as potential Culex pipiens L. larvicides, Bioorg. Chem. 154 (2025) 108090.
[37] G. Singh, B.S.Gill Heena, D. Baliyan, S. Gupta, S.C. Sahoo, Vikas, C. Espinosa-Ruíz, M.A. Esteban, Naked eye Fe (III) recognition and anticancer efficacy evaluation via diazenyl-propargyl appended imine functionalized moiety, J. Mol. Liq. 412 (2024) 125867.
[38] C.Y. Jia, J.Y. Li, G.F. Hao, G.F. Yang, A drug-likeness toolbox facilitates ADMET study in drug discovery, Drug Discov. Today 25 (1) (2020) 248–258.
[39] G. Singh, P. Malik, S. Khurana, Mithun, P. Markan, T. Diskit, K.N. Singh, B.S. Gill, D. Baliyan, Chalcone derived bis-organosilane and its magnetic nanoparticles: unveiling precision in selective Cu (II) ion detection and elucidating biocompatibility, Spectrochim. Acta Part A: Mol. Biomol. Spectrosc. 325 (2025) 125124.